Crystallographic study of self-assembled dysprosium silicide nanostructures on Si(001)

Gangfeng Ye,[1] Martin A. Crimp,[1] and Jun Nogami[2]
[1]*Chemical Engineering and Materials Science, Michigan State University, East Lansing, Michigan 48824, USA*
[2]*Department of Materials Science and Engineering, University of Toronto, Toronto, Ontario, Canada M5S 3E4*
(Received 11 October 2005; revised manuscript received 6 March 2006; published 28 July 2006)

The crystallography of epitaxial dysprosium silicide nanometer scale islands on Si(001) has been studied using transmission electron microscopy. Cross-sectional high resolution images show that the silicide nanostructures have either hexagonal or orthorhombic/tetragonal crystal structure. Moiré fringe patterns from plan view specimens show that elongated islands have the hexagonal structure while islands with smaller aspect ratios have the orthorhombic/tetragonal structure of $DySi_2$. Less lattice distortion and/or fewer dislocations are seen along the small lattice mismatch direction for both the hexagonal and orthorhombic/tetragonal silicides, indicating that lattice mismatch plays an important role in controlling island morphology.

DOI: 10.1103/PhysRevB.74.033104 PACS number(s): 68.55.Jk, 68.37.Lp, 68.55.−a

Several rare earth metal silicides form nanowires (NW) on silicon surfaces.[1–8] These NW are attractive objects for study since they have nanometer scale lateral dimensions, micron scale lengths, they show metallic conduction, and they can exhibit interesting one dimensional band structures.[9] It is generally agreed that these silicides form NW due to a lattice mismatch anisotropy between the silicides and the substrate.[2,3] For the case of dysprosium, when the hexagonal form of Dy disilicide ($DySi_2$) grows with the *a* and *c* axes parallel to the Si(001) surface along Si$\langle 1\bar{1}0\rangle$ directions, the mismatches with the substrate along the two perpendicular axes are small (−0.23%) and large (7.32%), respectively.[10] Consequently, the growth along the *a* axis is energetically preferred, while the growth is constrained along the *c* axis, resulting in NW formation.

In fact, during the initial stages of $DySi_2$ growth on Si(001), a variety of nanostructures are formed, and the terminology used to describe them varies in the literature. The nanostructures with the smallest cross section are highly elongated islands that are a single layer of silicide thick; we have referred to these structures as nanowires in our previous work, and we will call them one dimensional nanowires (1DNW) here.[3,7,9] It is also possible to grow highly elongated islands that are somewhat thicker (height >0.6 nm) and broader (width >5 nm) and composed of more than two or three atomic layers of silicide. These have also been called nanowires in the literature, and we refer to them here as three dimensional nanowires (3DNW).[2,5,6] Finally, there are also three dimensional silicide islands with much smaller aspect ratios (for convenience, these islands will be referred to as rectangular islands, and the 3DNW and rectangular islands collectively as 3D islands).[2–4,7,11] Much of the prior work on the rare earth (RE) silicide nanowires is in fact evenly split between 1DNW and 3DNW, with no particular distinction drawn between them. However, it is interesting to consider how they may differ, since the structure of a single silicide layer and multiple layers of silicide would be not necessarily be the same.

Further complicating the growth of 3D islands is the fact that in addition to the hexagonal phase, $DySi_2$ has two other polymorphic orthorhombic and tetragonal phases,[12] which have lower mismatch anisotropy with silicon.[10] It has been proposed that these other phases could form 3D islands with smaller aspect ratios than the 1DNW.[11,13] There has been no experimental verification of this supposition, although prior cross sectional transmission electron microscopy (TEM) results showing that $DySi_2$ 3D islands can consist of either the hexagonal phase or the orthorhombic phases.[4,14]

In this paper, we report both cross-sectional and plan view TEM data on a nanometer scale $DySi_2$ islands grown on Si(001), including both 3DNW and rectangular islands. Cross-sectional TEM data demonstrates that the hexagonal and the orthorhombic or tetragonal (orth/tet) phases coexist on the surface. Moiré fringe pattern analysis shows that the crystal structure of the 3DNW is hexagonal, while the rectangular islands are orth/tet. This result directly correlates the crystal structure, nanostructure morphology, and the lattice mismatch for the first time.

Silicide nanostructures were grown by evaporating Dy onto Si(001) substrates at elevated temperature (typically 600 °C) in an ultrahigh vacuum (UHV) chamber (base pressure 2.0×10^{-10} Torr) and annealed at 600 °C. Prior to deposition, the silicon substrates were repeatedly flashed up to 1175 °C to clean the surface. Metal coverage was determined by timed exposure to the source (whose evaporation rate was calibrated by a quartz crystal thickness monitor). Dy coverages ranged from 2 to 3 monolayers (ML). [1 ML $=6.78\times10^{14}$ atoms/cm^2=surface atomic density on Si(001)]. *In situ* STM images were taken at room temperature. Cross-sectional TEM samples were prepared by using the sandwich technique by sectioning perpendicular to the Si$\langle 110\rangle$ direction, while plan view samples were prepared by ion milling from the substrate side.[15] TEM imaging was carried out using a JEOL 2200FS operating at 200 kV.

Figure 1 shows typical scanning tunneling microscopy (STM) and plan view TEM images of $DySi_2$ growth morphology. In these images, both 1DNW and 3D islands (including 3DNW and rectangular islands) are present. Since the 1DNW are only a single layer thick, in the absence of any attempt to passivate them post growth, they are oxidized during *ex situ* TEM sample preparation. Therefore, it was not possible to acquire meaningful TEM data on the 1DNW, either in plan view or cross section.

Figures 2(a) and 2(b) show projections along the *a* and *c* axes of the hexagonal structure, respectively, while Fig. 2(c) displays the projection of the orth/tet structure along the *a* or *b* axis. Table I lists the bulk silicide lattice parameters for all three structures.

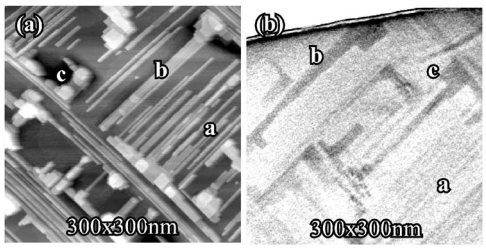

FIG. 1. Morphologies of $DySi_2$ samples showing three different nanostructure types: 1DNW, 3DNW, and rectangular islands, marked in the figure as *a*, *b*, and *c*, respectively. (a) is an STM image (b) is a plan view TEM image

Figure 3(a) shows a representative cross section of a portion of a 3DNW whose total length was at least ~0.5 μm. It displays a hexagonal arrangement of atoms, consistent with the projection along the *c* axis of hexagonal $DySi_2$ [Fig. 2(b)]. Lateral lattice parameter measurements from fast Fourier transform (FFT) analysis agree with the bulk hexagonal silicide values listed in Table I, meaning that there is no measurable lattice mismatch along the long axis of this island. This is consistent with the fact that there are no dislocations seen in this and any other such hexagonal silicide islands viewed along the *c* axis. These observations indicate the hexagonal phase grows very well along the *a* axis.

The atomic arrangement in Fig. 3(b) displays rectangular symmetry and is consistent with the hexagonal structure viewed along the *a* axis [Fig. 2(a)]. Once again, measured lateral lattice parameters agree with bulk values, and thus there is significant mismatch between silicide and substrate along the *c* direction. It is expected that the growth along the *c* axis is constrained. This is consistent with the observation that the width of the islands viewed along the *a* axis [Fig. 3(b)] ranged from 8 nm to 50 nm, which is very small compared to the width of the hexagonal silicide island in side view [Fig. 3(a)].

Figure 4 shows a $DySi_2$ island with a different crystal structure. There is a half atom column shift between every two horizontal atom rows, consistent with the orth/tet crystal structure [Fig. 2(c)]. Our lattice parameter measurements are

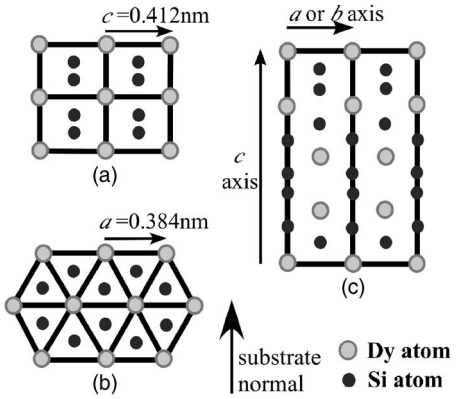

FIG. 2. Crystal models of bulk $DySi_2$ phases. (a) and (b) represent the projection of hexagonal $DySi_2$ along *a* and *c* axes. (c) shows projection of the orthorhombic/tetragonal structure along the *a* or *b* axis.

TABLE I. Summary of the lattice parameters of bulk $DySi_2$ phases and their corresponding mismatches with Si(001).

		Bulk lattice parameters (nm)			Mismatch with Si(001) (%)		
Structure	Prototype	*a*	*b*	*c*	*a*	*b*	*c*
Hexagonal	AlB_2	0.383		0.412	−0.23		7.32
Tetragonal	$ThSi_2$	0.403	0.403	1.338	4.95	4.95	
Orthorhombic	$GdSi_2$	0.404	0.395	1.334	5.21	2.73	

subject to 0.01 nm error, and so it is not possible to distinguish the orthorhombic and tetragonal structures in this study.

From Figs. 3 and 4, it is clear that the $DySi_2$ nanostructures take up either the hexagonal or orth/tet forms. Although the cross section shown in Fig. 3(a) suggests that the hexagonal crystal structure is associated with 3DNW, our cross sectional data taken as a whole does not unambiguously relate the crystal structures of the nanostructures to their morphology, since the cross-sectional width of 3DNW can fall in the same range as that of the rectangular islands, as is evident from plan view images (Fig. 1).

It is known that moiré fringe patterns are very sensitive to lattice mismatch and are well suited for evaluating the structural relationships between the moiré target ($DySi_2$ nanostructures) and the moiré reference (silicon substrate). The moiré fringe spacing is (assuming no rotation between the silicide and the silicon): $D_{\text{moire fringe}}=\frac{d_{DiSi_2}d_{Si}}{d_{Si}-d_{DySi_2}}$, where d_{Si} is the substrate lattice periodicity, d_{DySi_2} is the silicide lattice periodicity, and the $D_{\text{moire fringe}}$ is the moiré fringe spacing.[16] Based on this formula and the bulk silicide lattice parameters, the calculated moiré fringe spacings of the different $DySi_2$ phases on Si(001) are listed in Table II. According to the table, hexagonal silicide islands should have a large moiré fringe spacing of 82 nm along the small lattice mismatch direction and a small fringe spacing of 2.8 nm in the large lattice mismatch direction, resulting in a stripe-like (striped) appearance. The lattice mismatch is similar in both Si⟨110⟩ directions for the orth/tet phase, and should result in a mesh-like (meshed) appearance with similar moiré fringe spacings in perpendicular directions.

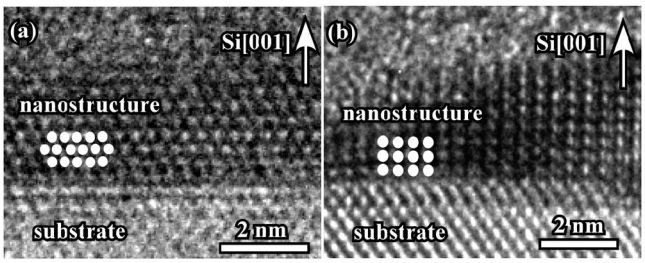

FIG. 3. Cross-sectional high resolution TEM images of a hexagonal $DySi_2$ nanostructure, viewed along the *c* axis (a) and along the *a* axis (b). Hexagonal symmetry is seen in (a) and rectangular symmetry is seen in (b).

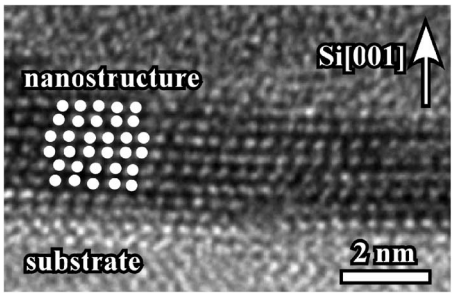

FIG. 4. Side view cross sectional high resolution TEM image of orth/tet nanostructure

Moiré patterns of these two general types were observed in plan view TEM. Figure 5(a) shows a meshed pattern, with fringe spacings from 3.2 nm to 6.9 nm, with the fringe spacing varying for different islands. Striped moiré fringes with spacings of 2.4–3.2 nm are evident in Fig. 5(b). The measurement error is about 20%. The measured moiré fringe spacings are also included in Table II, and are consistent with the calculated values. Striped moiré fringe patterns were typically observed on elongated 3D islands, and meshed patterns were only found on rectangular 3D islands, indicating that as the aspect ratio decreases, the orth/tet phase becomes dominant.

It might be suggested that the features we are identifying as moiré fringes are in fact dislocation networks. Mismatched interfaces will have interfacial dislocations that accommodate the mismatch strains. These dislocation will have spacings directly resulting from the lattice mismatch, $D = b/\delta$, where b is the magnitude of the interfacial dislocations and δ is the mismatch. The Burgers vector will depend on the details of the silicide and silicon. For example, for interfacial dislocations with line directions along the **a** direction of the hexagonal silicide, the dislocations will consist of 2 half planes in the silicon ($\mathbf{b}=1/2\langle 110\rangle$), as illustrated in Fig. 6. Dissociation of this dislocation in to partials is unlikely as no stable dissociations of $\frac{1}{2}\langle 110\rangle$ dislocations have been observed on {001} planes in Si. Consequently, based on the mismatch between the Si and silicide, the spacing of the $\frac{1}{2}\langle 110\rangle$ dislocations will be 5.25 nm which is double the observed fringe spacing. Moreover, no regular arrays of dislocations are seen in the cross sectional TEM images.[4] The

TABLE II. A comparison of the calculated and measured moiré fringe spacings of $DySi_2$ on Si(001). The calculated spacings are based on bulk lattice parameters and zero rotation between the silicide and the silicon.

	Calculated fringe spacing (nm)			Measured fringe spacing (nm)		
Structure	*a*	*b*	*c*	*a*	*b*	*c*
Hexagonal	82		2.8	>90		2.4–3.2
Tetragonal	4.1	4.1		3.2–6.9		
Orthorhombic	3.9	7.2				

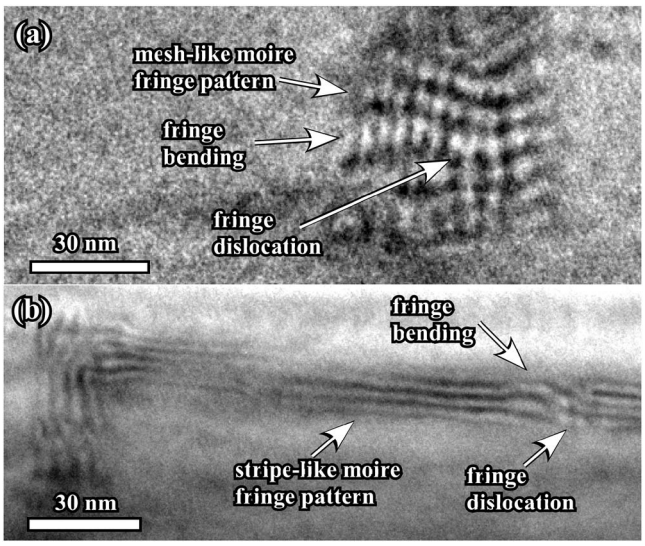

FIG. 5. Plan view TEM reveals mesh-like moiré fringe patterns on rectangular $DySi_2$ 3D islands, as shown in (a), and stripe-like moiré fringe pattern on elongated 3D islands, as shown in (b). This indicates that square 3D islands have an orthorhombic/tetragonal form and elongated 3D islands have a hexagonal form. Fringe bending and dislocations are marked.

dislocations that are seen are irregularly spaced, in contrast to the comparative regularity in the plan view fringe spacing. To reiterate, the observed fringes are fully consistent with the formation of moiré fringes due to the diffraction from the {220} planes in the Si interfering with {0002} diffraction from the silicide.

Moiré fringe patterns can also be used to provide information on lattice distortion and dislocations.[16] The bending of the moiré fringes indicates nonuniform lattice strain in the target material ($DySi_2$ nanostructures in this case), while edge dislocations in the moiré fringe give a one-to-one correspondence to edge dislocations in the target material. The distorted appearance of the mesh patterns seen in rectangular

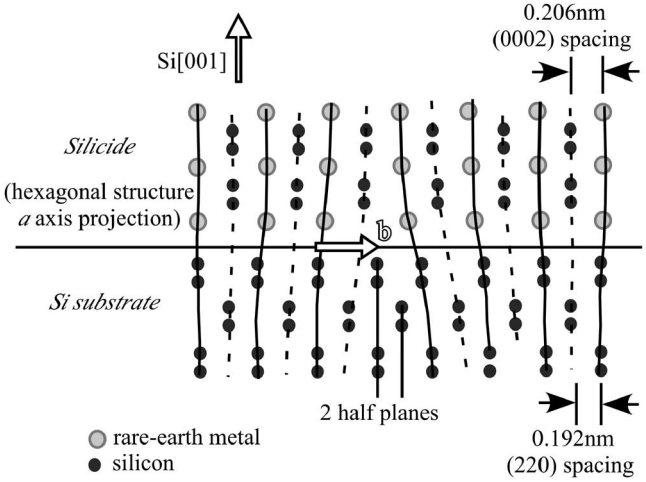

FIG. 6. Schematic of an edge dislocation in the hexagonal silicide with a Burgers vector of $\mathbf{b}=1/2\langle 110\rangle$ oriented parallel to the interface.

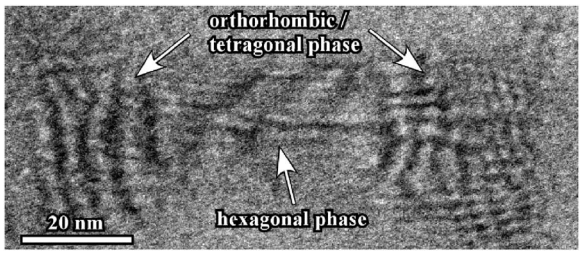

FIG. 7. The coexistence of the orth/tet and hexagonal phases. Meshed fringes indicative of the orth/tet phase are seen on both ends, while stripes in the central part indicate the hexagonal phase.

3D islands in Fig. 5(a), indicates significant lattice distortion and/or some dislocations, which are also seen in cross sectional images of orth/tet islands.[4] These distortions occur because the lattice mismatch (2.73%–5.21%) introduces significant strain near the interface, even if silicide layers in the remainder of the island are relaxed. In contrast, the hexagonal phase 3D island shown in Fig. 5(b) indicates mild fringe bending and only a few dislocations along the length. This is consistent with the small lattice mismatch (−0.23%) along the length of the elongated island, resulting in the limited stress accumulation during hexagonal island growth.

Two silicide phases can coexist in an individual nanostructure. Figure 7 shows a short rectangular island with both ends having the orth/tet structure and the central section having the hexagonal structure. While it is possible that this particular structure might arise from coalescence of separate islands, these dumbbells consisting of a hexagonal island terminated in blocks of orth/tet are quite commonly seen in our STM images, and so this suggests the possibility that they form due to a transformation from one phase to the other. Such a transformation can be accomplished through the formation of a series of stacking faults (see Houssay *et al.* for a description of the stacking of these phases).[17] Our prior STM studies have shown that 1DNW are transformed to the larger 3D islands by extended post growth annealing, but only 1DNW are present if the sample is quenched immediately after the end of Dy deposition.[11] Moreover, the 3D islands are either entirely rectangular, or elongated with a rectangular portion attached somewhere along their length. Hence, it would appear that the hexagonal silicide phase dominates nucleation, but the ort/tet phase associated with rectangular 3D islands is more thermodynamically stable at the growth temperature. As the orth/tet phase is associated with larger 3D islands, it most likely has a lower volume free energy that dominates the effects of interfacial strain at larger sizes.

To summarize, high resolution TEM analysis from cross-sectional $DySi_2$ samples demonstrates that both hexagonal and orth/tet phase silicide nanostructures are present. Moiré fringe patterns from plan view TEM samples shows that elongated 3D islands (3DNW) are the hexagonal phase and rectangular 3D islands are the orth/tet phase. All of the analyses support the contention that $DySi_2$ nanostructure growth is dominated by lattice mismatch. The hexagonal phase $DySi_2$ nanostructures grows very well along the *a* axis and only a small amount of crystal distortion and dislocations are observed. This is consistent with the expected anisotropic lattice mismatch growth. For the orth/tet phase, large amounts of lattice distortion were observed inside of the islands due to their significant biaxial lattice mismatch. During $DySi_2$ nanostructure growth, the hexagonal and orth/tet phases may coexist in one nanostructure, which indicates that one phase may transform to the other.

This work is supported by NSF DMR-0305472. The JEOL 2010F TEM was acquired in part by funds from NSF grant DMR-0079578. J.N. acknowledges support from the National Sciences and Engineering Research Council of Canada.

[1] C. Preinesberger, S. Vandre, T. Kalka, and M. Dahne-Prietsch, J. Phys. D **31**, L43 (1998).
[2] Y. Chen, D. A. A. Ohlberg, G. Medeiros-Ribeiro, Y. A. Chang, and R. S. Williams, Appl. Phys. Lett. **76**, 4004 (2000).
[3] J. Nogami, B. Z. Liu, M. V. Katkov, C. Ohbuchi, and N. O. Birge, Phys. Rev. B **63**, 233305 (2001).
[4] G. Ye, J. Nogami, and M. A. Crimp, Thin Solid Films **497**, 48 (2006).
[5] Z. He, M. Stevens, D. J. Smith, and P. A. Bennett, Appl. Phys. Lett. **83**, 5292 (2003).
[6] J. C. Chen, G. H. Shen, and L. J. Chen, Appl. Surf. Sci. **142**, 291 (1999).
[7] Y. Chen, D. A. A. Ohlberg, and R. S. Williams, J. Appl. Phys. **91**, 3213 (2002).
[8] C. Ohbuchi and J. Nogami, Phys. Rev. B **66**, 165323 (2002).
[9] H. W. Yeom, Y. K. Kim, E. Y. Lee, K.-D. Ryang, and P. G. Kang, Phys. Rev. Lett. **95**, 205504 (2005).
[10] K. Maex and M. Rossum, *Properties of Metal Silicides* (INSPEC, London, 1995).
[11] B. Liu and J. Nogami, J. Appl. Phys. **93**, 593 (2003).
[12] T. B. Massalski, H. Okamoto, P. R. Subramanian, and L. Kacprzak, *Binary Alloy Phase Diagrams* (ASM International, Metals Park, OH, 1990).
[13] B. C. Harrison and J. J. Boland, Surf. Sci. **594**, 93 (2005).
[14] Z. He, D. J. Smith, and P. A. Bennett, Phys. Rev. B **70**, 241402(R) (2004).
[15] J. C. Bravman and R. Sinclair, J. Electron Microsc. Tech. **1**, 54 (1984).
[16] D. B. Williams and C. B. Carter, *Transmission Electron Microscopy* (Plenum Publishing Corporation, New York, 1996).
[17] E. Houssay, A. Rouault, O. Thomas, R. Madar, and J. P. Senateur, Appl. Surf. Sci. **38**, 156 (1989).